

Solvent-Controlled Synthesis of Highly Luminescent Carbon Dots with a Wide Color Gamut and Narrowed Emission Peak Widths

Hui Ding, Ji-Shi Wei, Peng Zhang, Zi-Yuan Zhou, Qing-Yu Gao, and Huan-Ming Xiong*

Carbon dots (CDs) have tremendous potential applications in bioimaging, biomedicine, and optoelectronics. By far, it is still difficult to produce photoluminescence (PL) tunable CDs with high quantum yield (QY) across the entire visible spectrum and narrow the emission peak widths of CDs close to those of typical quantum dots. In this work, a series of CDs with tunable emission from 443 to 745 nm, quantum yield within 13–54%, and narrowed full width at half maximum (FWHM) from 108 to 55 nm, are obtained by only adjusting the reaction solvents in a one-pot solvothermal route. The distinct optical features of these CDs are based on their differences in the particle size, and the content of graphitic nitrogen and oxygen-containing functional groups, which can be modulated by controlling the dehydration and carbonization processes during solvothermal reactions. Blue, green, yellow, red, and even pure white light emitting films (Commission Internationale de L'Eclairage (CIE)= 0.33, 0.33, QY = 39%) are prepared by dispersing one or three kinds of CDs into polyvinyl alcohol with appropriate ratios. The near-infrared emissive CDs are excellent fluorescent probes for both *in vitro* and *in vivo* bioimaging because of their high QY in water, long-term stability, and low cytotoxicity.

cytotoxicity, especially the amazing photoluminescence (PL).^[6–9] However, the PL mechanisms of CDs are controversial and the formation processes of CDs also remain unclear. It is still a great challenge to modulate the fluorescence properties of CDs across the entire visible spectrum till the near infrared (NIR) region. By far, there are few successful reports concerning tunable PL of CDs from blue to red. For example, Fan et al. obtained PL-tunable CDs through heating treatment of ethanol solution of citric acid and diammonaphthalene isomers.^[10] Bao et al. synthesized PL-tunable CDs with emission ranging from blue to orange by wet oxidation of carbon fibers.^[11] Our group also synthesized multicolor CDs from blue to red in one pot and separated them through a column chromatography.^[12] Although bright PL-tunable CDs have been obtained in these pioneering works, the optimal PL peaks were not in the deep-red or NIR

1. Introduction

Carbon dots (CDs), as a new kind of luminescent material, have drawn extensive attention during the past decade.^[1–5] Scientists have made great efforts to develop this material, and now, CDs can be easily fabricated from abundant low-cost sources with green methods, and exhibit excellent photostability and low

region. Furthermore, the time-consuming separation/purification techniques such as dialysis and chromatography are always necessary. In another study, Hu et al. prepared a series of multicolor fluorescent CDs with PL peak varying from 400 to 710 nm, but the QY of the red emissive CDs is only 5% and the synthetic process is sophisticated with a poor controllability.^[13] Since the practical applications, including the animal imaging *in vivo* and the white light emitting diodes, require bright full-color emission from blue to NIR,^[14–17] it is important and urgent to develop a facile, high-yield route to prepare PL-tunable CDs with high QY across the entire visible spectrum. In addition, the narrowed FWHM is highly required for increasing both the background-probe fluorescence contrast of bioimaging and the color saturation of light emitting devices.^[9,18]

To this aim, the relationships between the typical excitation dependent/independent emission features and the complicated structures/compositions of CDs should be understood deeply, which involve the particle sizes, the sp² carbon framework, the graphitization degree, the heteroatom doping, organic groups, surface states, etc.^[19–21] Several research groups have prepared CDs with gradually tuned optical properties by varying carbon sources and reaction conditions, and tried to correlate the PL features of CDs with their particle sizes, element contents, and functional groups. For instance, Lin et al. produced three kinds of CDs with red-shifted emission and improved PL QY through

Dr. H. Ding, Prof. Q.-Y. Gao
School of Chemical Engineering and Key Laboratory of Coal Processing and Efficient Utilization of Ministry of Education
China University of Mining and Technology
Xuzhou 221116, Jiangsu, P. R. China

Dr. J.-S. Wei, Dr. P. Zhang, Prof. H.-M. Xiong
Department of Chemistry and Shanghai Key Laboratory of Molecular Catalysis and Innovative Materials
Fudan University
Shanghai 200433, P. R. China
E-mail: hmxiong@fudan.edu.cn

Dr. Z.-Y. Zhou
School of Chemical Biology and Biotechnology
Shenzhen Graduate School of Peking University
Shenzhen 518055, China

 The ORCID identification number(s) for the author(s) of this article can be found under <https://doi.org/10.1002/smll.201800612>.

DOI: 10.1002/smll.201800612

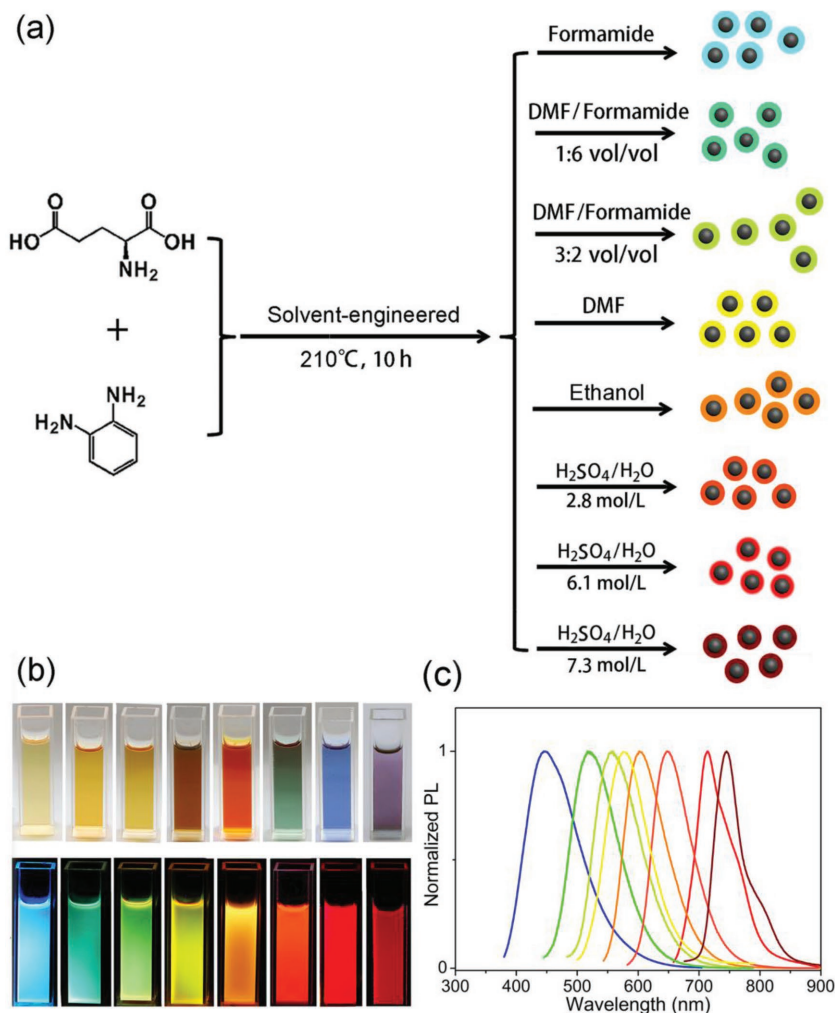


Figure 1. a) A solvent-engineered strategy for synthesis of multicolor fluorescent CDs using L-glutamic acid and o-phenylenediamine as starting materials. b) Photos of the as-prepared CDs in daylight (upper) and UV light (bottom), respectively. c) Normalized PL emission spectra of all the above samples under excitation of 365 nm.

increasing their particle size and nitrogen content.^[22] Sun et al. synthesized a series of CDs with multiple color emission by controlled graphitization and surface functionalization.^[23] Yang et al. obtained blue and red emitting CDs by varying the reaction temperature and indicated that C=O and graphitic N play important roles of the red emission.^[24] Qu et al. reported full-color emission CDs by tuning the solvents in solvothermal conditions and demonstrated that the increased sizes of CDs determine their tunable emission colors.^[25] These instructive works imply that both the carbon cores and surface states determine the optical performances of CDs, so that optimizing the dehydration reaction between precursors and adjusting the graphitization degree of CDs will produce CDs with desired PL properties. To the best of our knowledge, by far, there is no report involving highly efficient PL-tunable CDs with significantly narrowed FWHM over the entire visible spectrum by controlling their growth processes, which is very important for interpreting both the formation processes and the PL mechanisms of CDs.

Herein, we report a novel solvent-controlled synthetic route to obtain highly luminescent CDs with PL emission across the entire visible region and gradually narrowed FWHM. Only by changing the solvent in reactions, we modulated the particle size and graphitic nitrogen content of CDs in a wide range successfully, and found that the solvent controls the dehydration and carbonization processes under solvothermal conditions. The optimal sample has a NIR emission at about 715 nm, with a QY of 43% in ethanol and a QY of 36% in water, which are the highest values for the NIR-emitting CDs at present. The detailed characterizations proved that the energy gap and emission efficiency of CDs correlate with their particle sizes and graphitic nitrogen contents, and the narrowed, excitation-independent luminescence mainly originate from their surface states. These CDs can be mixed with polyvinyl alcohol (PVA) matrix to form blue, green, yellow, red, and pure white light emitting films. They can also be employed as luminescent probes for bioimaging both in vitro and in vivo with extremely low toxicity and long-term stability.

2. Results and Discussion

Our CDs are synthesized solvothermally by heating a mixture of L-glutamic acid and o-phenylenediamine in four different solvents (formamide, dimethylformamide, ethanol, and aqueous H₂SO₄ solution) and their combinations with appropriate ratios, respectively, which show tunable PL emission from blue to NIR (Figure 1a). Both precursors are selected carefully and the optimal ratio is applied for each reaction. Such dehydration reaction under supercritical conditions is favorable to form conjugated sp²-domains and dope nitrogen into the domains. After solvothermal treatment at 210 °C for 10 h followed by precipitation and separation, eight solid samples are obtained and then redispersed in ethanol for characterizations. These ethanol solutions have different colors in the daylight, and show tunable PL emission from blue to NIR under a UV light of 365 nm (Figure 1b). Their PL emission maxima locate at 443, 515, 544, 571, 594, 640, 715, and 745 nm, respectively, covering the entire visible spectrum (Figure 1c). Four typical CD samples with blue, green, yellow, and red fluorescence are chosen for further characterizations, which are labelled as B-CDs, G-CDs, Y-CDs, and R-CDs, respectively.

The UV-vis absorption spectra of the four selected samples in Figure 2 exhibit significant absorption in both the UV and the visible regions. In the UV region, two peaks are observed at 268 and 277 nm respectively, corresponding to the π - π^* transitions of C=C and C=N bonds in carbon cores.^[12] Their

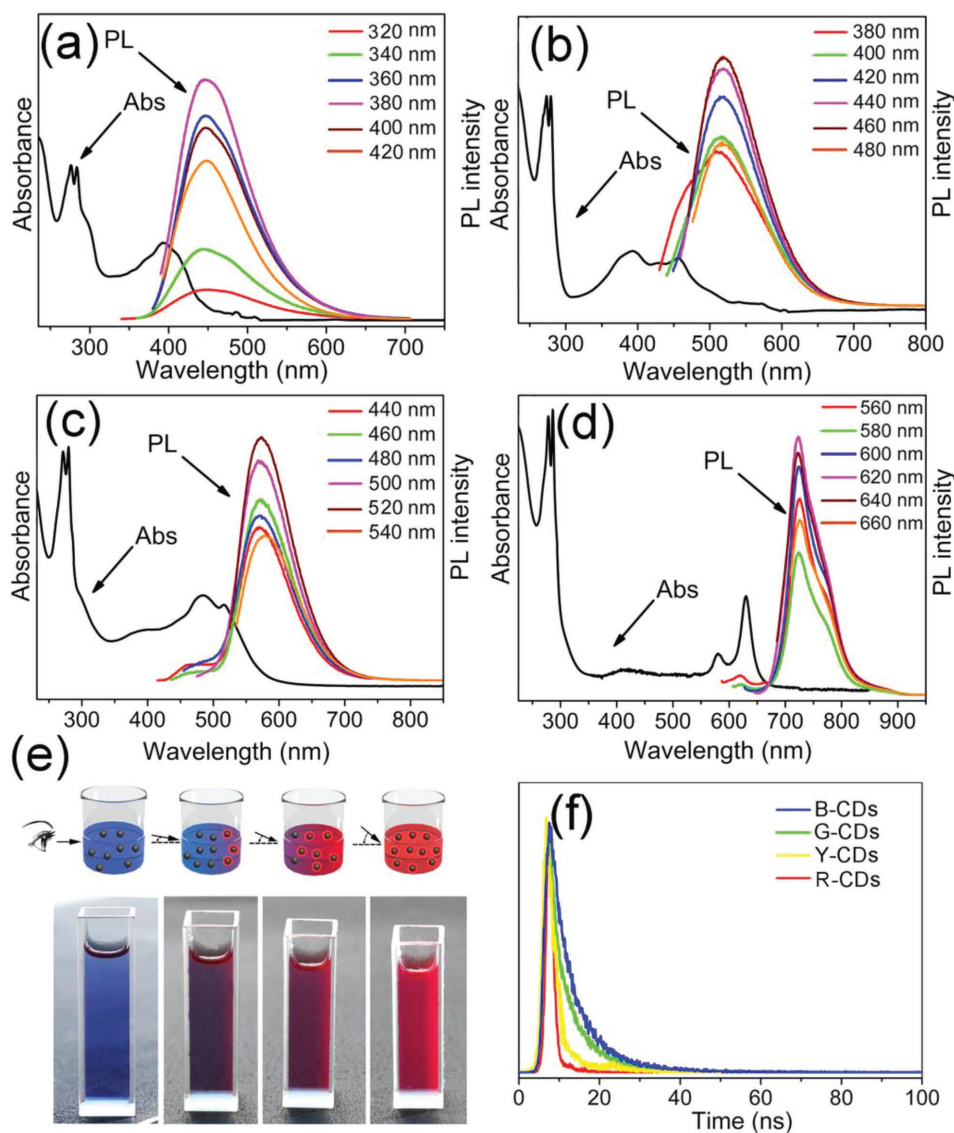


Figure 2. Absorption spectra and PL emission spectra of a) B-CDs, b) G-CDs, c) Y-CDs, and d) R-CDs under excitation of different wavelengths of light (see the inset legends). e) An R-CDs solution exhibits different colors varying from blue to red when observed from different angles (upper), and the corresponding photos of the same R-CD solution under sunlight (bottom). f) Time-resolved PL spectra of the four selected samples.

absorption intensity increase from B-CDs to R-CDs, implying a gradually increasing content of the nitrogen-doped aromatic rings in carbon cores.^[26] However, in the lower-energy region, four samples display distinct absorption bands at 389, 456, 512, and 634 nm, respectively, indicating that these samples possess different surface states.^[27–29] Similar to many other reported CDs,^[30,31] our CDs also show excitation-independent PL emissions, i.e., their PL emission peaks do not shift when the excitation wavelength changes. The absolute QYs for B-, G-, Y-, and R-CDs are determined to be 54%, 41%, 51%, and 43% respectively, using an integrating sphere under their optimal excitation wavelengths (Table S1, Supporting Information). It is very interesting that the R-CDs solution color turns from blue to red in sunlight when observed from different angles, which is rarely seen in the literature about CDs, but common in organic dye solution like rhodamine (Figure S1, Supporting Information),

confirming their high QY and strong absorption in the visible region (Figure 2e).^[28] The time-resolved PL decay curve of each sample was also measured. The results (Figure 2f; Table S2, Supporting Information) show that they can be fitted by a dual-exponential formula, involving a short-lived component τ_1 (about 1 ns) and a long-lived component τ_2 (about 10 ns), which are assigned to the recombination processes in the core states and the surface states, respectively.^[32,33] It is clear that from B-CDs to R-CDs, as the average lifetime decreases from 10.2 to 2.1 ns, the τ_1 proportion increases from 40% to 88%, indicating that the role of core states in the radiative lifetime of these CDs increases with their PL redshift.^[26,34] The above results demonstrate that our CDs possess excellent and uniform optical properties, and their tunable PL emission can be ascribed to both the carbon cores and the surface states which are controlled by different reaction solvents.

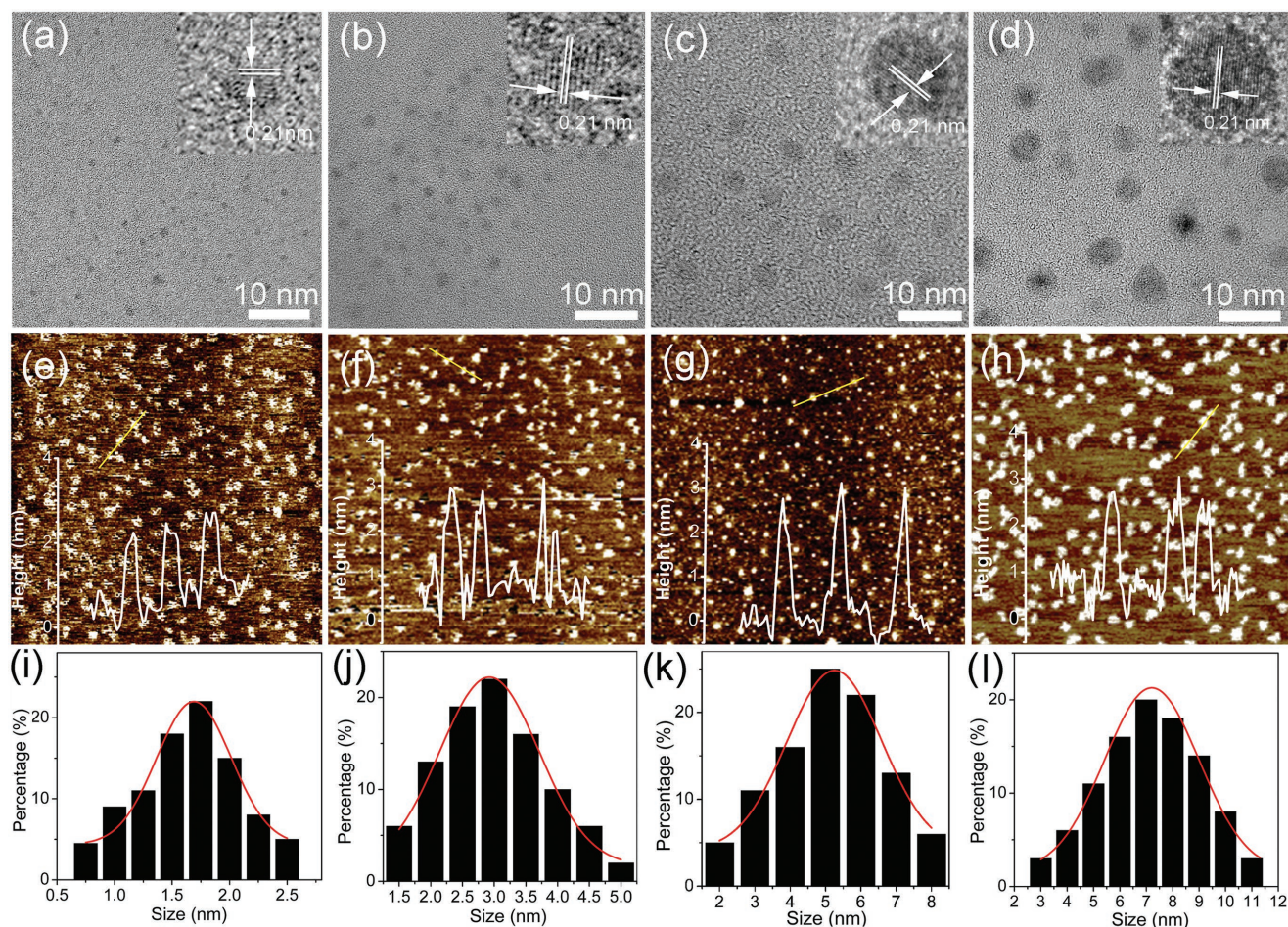


Figure 3. TEM and HRTEM images (inset) of a) B-CDs, b) G-CDs, c) Y-CDs, and d) R-CDs. AFM images of e) B-CDs, f) G-CDs, g) Y-CDs, and h) R-CDs. Particle size distribution diagrams of i) B-CDs, j) G-CDs, k) Y-CDs, and l) R-CDs. White lines are the height-profiles analysis along the corresponding lines in Figure 2e–h.

The four typical CDs are examined by transmission electron microscopy (TEM) and atomic force microscopy (AFM) to study their sizes and morphologies. In **Figure 3a–d**, the TEM images reveal that these CDs are homogeneous and well-dispersed, with average particle sizes of about 1.8, 3.1, 5.2, and 7.6 nm for B-, G-, Y-, and R-CDs, respectively. The high-resolution TEM (HRTEM) images show that all samples have similar well-resolved lattice fringes with a spacing of 0.21 nm, attributed to the (100) lattice distance of the graphitic carbon.^[35,36] The X-ray diffraction (XRD) patterns (Figure S2, Supporting Information) exhibit a broad peak at around 25.5° with enhanced intensity, indicating that the graphitization degree of samples increases from B-CDs to R-CDs gradually.^[37] The AFM images (Figure 3e–h) also show that these CDs are monodispersed, with a similar thickness of about 2.5–3.0 nm, corresponding to 5–6 layers of graphene.^[38] The Raman spectra of the four samples (**Figure 4**) show two peaks at 1348 and 1587 cm⁻¹, corresponding to the disordered structures or defects (D band) and the graphitic carbon domains (G band), respectively. The intensity ratios I_D/I_G are 1.18, 1.04, 0.87, and 0.73 for B-, G-, Y-, and R-CDs, respectively, suggesting a gradual increase in the size of sp²-domains,^[39,40] which is consistent with the above TEM and XRD results.

The compositions of these samples are investigated by Fourier transform infrared (FT-IR) spectra and X-ray photoelectron spectroscopy (XPS). In **Figure 5**, the FT-IR spectra show that these CDs possess abundant polar functional groups, such as O–H/N–H at 3444 cm⁻¹, C=O at 1677 cm⁻¹ and C–O at 1131 cm⁻¹, thereby guaranteeing their excellent solubility in polar solvents.^[41] From B-CDs to R-CDs, both the stretching vibration intensities of C=N at 1574 cm⁻¹ and C=C at 1503 cm⁻¹ gradually increase while the stretching vibration intensity of C=O at 1677 cm⁻¹ decreases significantly, indicating that the content of the nitrogen-doped polyaromatic structures is improved gradually through the dehydration reaction.^[28] In Figure S3 (Supporting Information), the full XPS spectra display three typical peaks at 285, 400, and 531 eV for C1s, N1s, and O1s, respectively, indicating that all the CDs consisted of the same elements. In the high-resolution XPS spectra (**Figure 6**), the C1s band can be deconvoluted into four binding energy peaks at 284.4, 285.6, 286.6, and 287.7 eV, which could be assigned to C–C/C=C, C–N, C–O, and C=O, respectively. The N1s spectra display three peaks at 398.4, 399.3, and 400.4 eV, attributed to pyridinic N, pyrrolic N, and graphitic N, respectively. The O1s spectra contain two peaks at 531.5 and 533.1 eV for

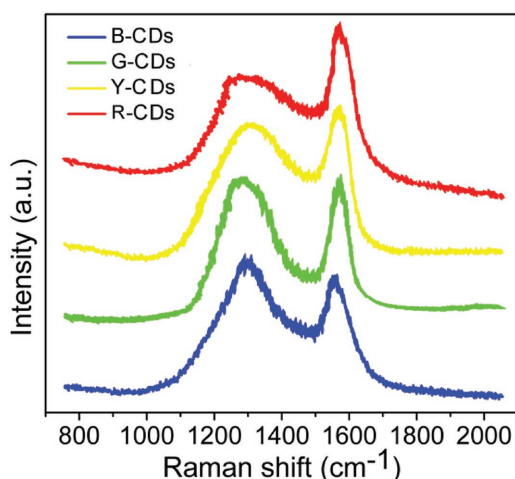


Figure 4. Raman spectra of the four selected CDs.

C=O and C–O bands, respectively.^[12] The atomic ratio between oxygen and carbon decreases from 19.78 (B-CDs) to 7.37% (R-CDs) (Table S3, Supporting Information), suggesting an increasing degree of graphitization in these CDs. Moreover, the sp^2 carbon content gradually increases from 0.26 (B-CDs) to 0.47 (R-CDs) as the graphitic N content also increases from 0.23 (B-CDs) to 0.44 (R-CDs), implying an increase in the size of sp^2 -conjugated domains in these CDs after the dehydration reaction (Table S4, Supporting Information), which agrees well with their increased particle size and graphitization degree. In brief, our CDs have large conjugated sp^2 domains with abundant oxygen/nitrogen-containing surface groups, and both their particle sizes and graphitic nitrogen contents increase concurrently when their PL emission shift from blue to red.

To explore the formation mechanism of the CDs, control experiments were carried out for synthesizing R-CDs in which only the reaction time and the H_2SO_4 concentration are tuned respectively. For the time-dependent experiments, the products collected after 1–7 h were analyzed by TEM (Figure S4, Supporting Information). At the initial reaction stage, the newly formed crosslinking molecules are amorphous and unclear. Then they agglomerate and become darker and darker and finally the carbonized nanoparticles come into being. This formation process indicates that the dehydration reactions among the precursors produce polymer dots first, and then the polymer dots turn into CDs (Scheme 1). And thus, the particle size and graphitization degree of CDs highly depends on the dehydration and carbonization conditions.^[25] From formamide to ethanol, the boiling point of the solvents decreases gradually, indicating the vapor pressure of the reactants at 210 °C increases in the same sequence, and the degree of dehydration and carbonization processes improve as well. When H_2SO_4 is employed, the dehydration reaction and carbonization process are accelerated due to the catalysis of H_2SO_4 , which yields NIR-emitting CDs with the largest size and the highest content of graphitic nitrogen. For the H_2SO_4 -dependent experiments, the H_2SO_4 concentration was tuned from 0.06 to 18.4 mol L^{-1} (the undiluted 98 wt% H_2SO_4). In Figure S5 (Supporting Information), when the concentration increases from 0.06 to 8.2 mol L^{-1} , the particle size of CDs gradually increases from 5.4 to 8.3 nm,

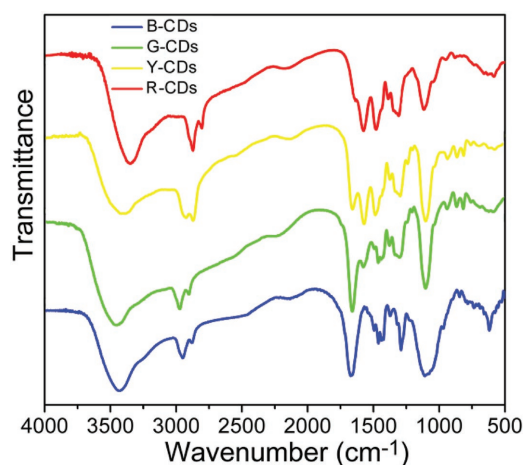


Figure 5. FT-IR spectra of the four selected CDs.

and the graphitization degree of CDs also increases. In the meantime, the PL emission of these samples redshifts from 581 to 756 nm (Figure S6, Supporting Information). However, when the higher concentrations of sulfuric acid were employed, the obtained CDs became smaller and smaller, which may be ascribed to the oxidation etching effects of concentrated H_2SO_4 (Figure S5, Supporting Information).^[11] And the as-prepared CDs show excitation-dependent PL behaviors in Figure S6 (Supporting Information). It should be mentioned that the largest CDs sample (Figure S5d, Supporting Information) has a QY of 3.7%, although it shows the mostly red-shifted emission, indicating that the surface groups of CDs would be destroyed due to excessive carbonization induced by concentrated H_2SO_4 .^[42] Our exploration to control the PL emission of CDs by tuning solvents in reactions not only suggests a new formation mechanism, but also points out a direction to design synthetic conditions and expand CDs emission to NIR windows.

To date, two popular models, including the carbon core state and surface state, have been proposed for elucidating the PL mechanisms of CDs.^[1,34] In previous reports, the PL redshift of CDs was always ascribed to their increasing contents of oxygen or nitrogen.^[12,43] However, in our case, both the nitrogen and oxygen contents measured by XPS do not show such relationship with the PL redshift of CDs (Table S3, Supporting Information). The XPS results show the graphitic nitrogen content increases as the PL redshifts (Table S4, Supporting Information), while the TEM and AFM results confirm the PL emission of CDs depends on the particle sizes and the sp^2 -conjugated domains heavily. It has been reported that the surface states of CDs is based on the synergistic hybridization between the carbon backbones and the connected functional groups, while the luminescent centers, where electrons and holes recombine to emit fluorescence, correlate with the extent of the π -electron conjugation and the content of graphitic nitrogen.^[11,20] The larger π -electron system or the higher graphitic nitrogen content will result in the narrower energy gap, so as to shift the PL emission to the red region. As another proof, the theoretical calculations based on density functional theory note that the band gap between the highest occupied molecular orbital and the lowest unoccupied molecular orbital narrows when the particle size increases or the graphitic

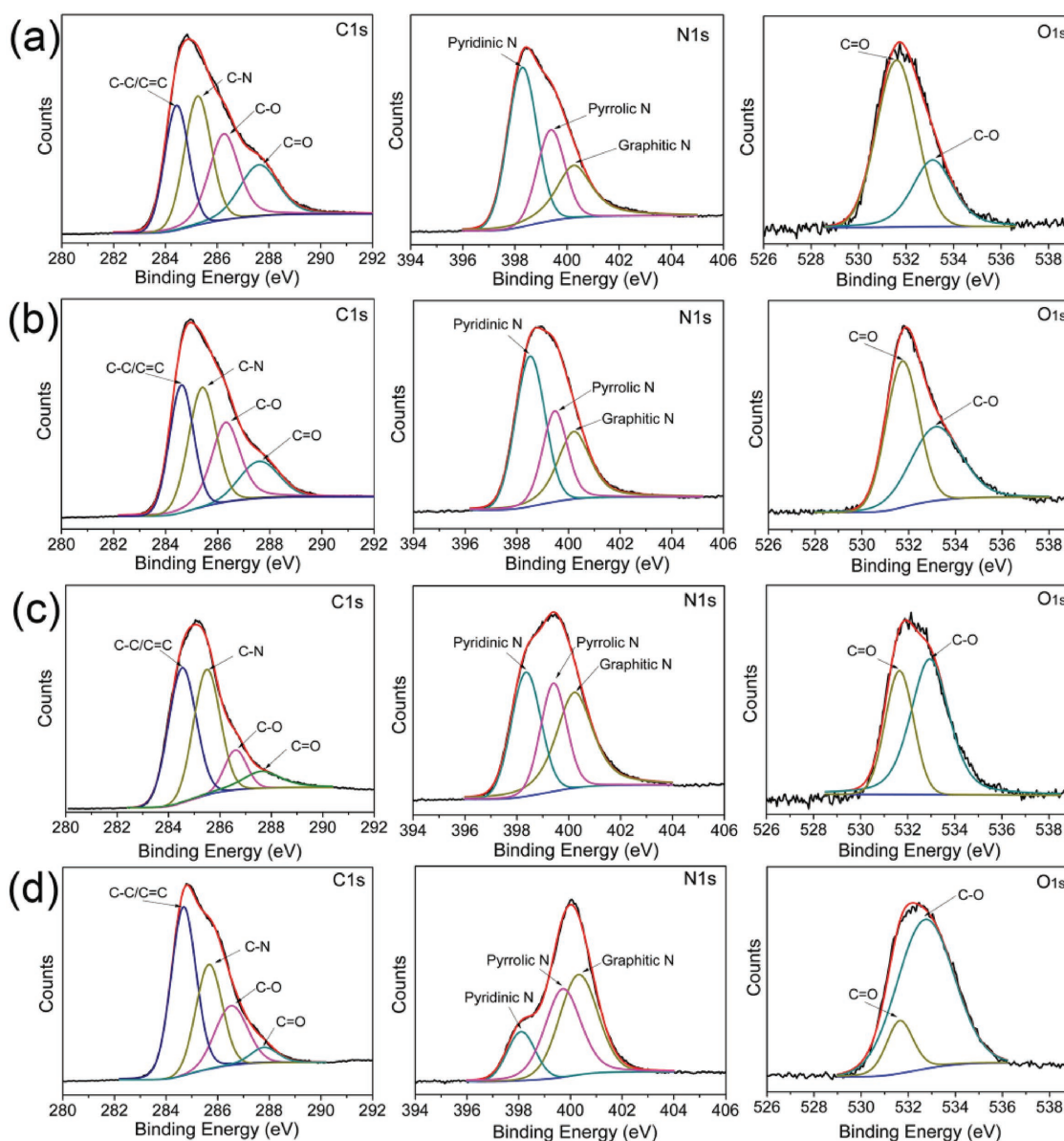
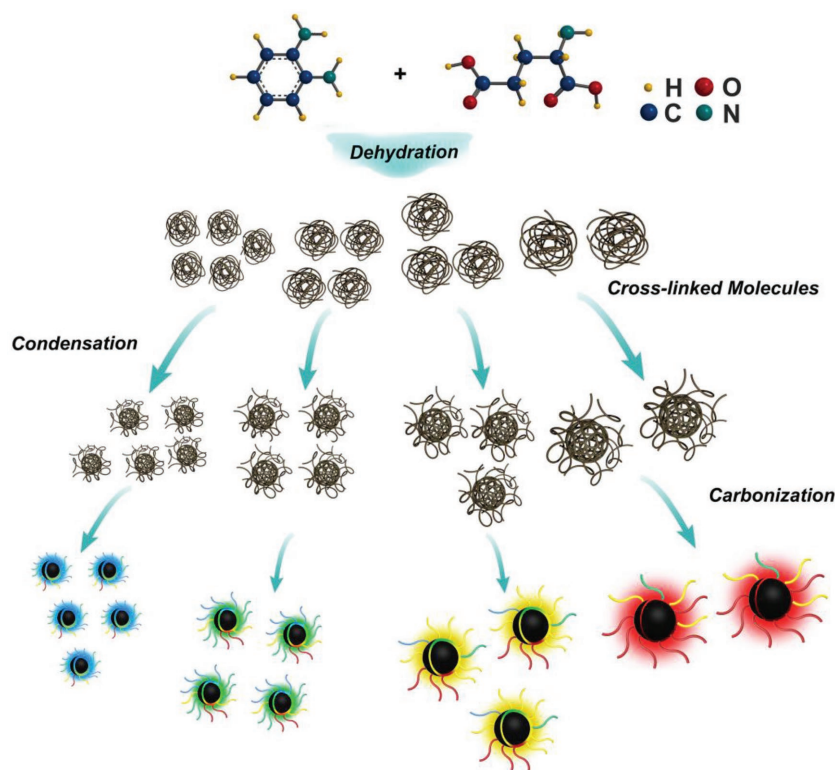


Figure 6. High-resolution XPS C 1s, N 1s, and O 1s spectra of a) B-CDs, b) G-CDs, c) Y-CDs, and d) R-CDs.

nitrogen content improves.^[23,44] Based on these results and conclusions, we believe that the PL emission of our CDs is based on surface-states, and that their energy gaps are modulated by both the π -electron system and graphitic nitrogen content. As a result, by accelerating the dehydration reaction and carbonization processes between L-glutamic acid and *o*-phenylenediamine, PL of CDs can be tuned accordingly from blue to NIR. Meanwhile, with the decrease of C=O, C-OH, and C-O-C groups in CDs, the recombination possibility of electrons and holes, captured by oxygen-related surface defects, is also decreased,^[13,45] thus exhibiting a narrowed FWHM from 108 to 55 nm in PL emission spectra of CDs (Table S1, Supporting Information), which is close to those of the typical QDs.^[46] As a proof to the contrary, PL emission curves with increased FWHM were observed again when these CDs were oxidized (Figure S6, Supporting Information). To further confirm the PL of the CDs

is based on their surface states, their pH-dependent behaviors are investigated. In Figure S7 (Supporting Information), all samples exhibit the maximal PL emission intensities under neutral conditions and their PL peaks red-shift as the pH value decreases, which are the typical surface-state controlled PL behaviors as reported in literature.^[12] Interestingly, the PL QYs of our CDs do not decrease distinctly as their particle size increase, which is inconsistent with the typical surface-state controlled emission, suggesting that the improved contents of graphitic nitrogen atoms within carbon cores make a significant contribution to the PL QYs. The graphitic nitrogen content is able to enhance the rigidity of the domains, so as to reduce the non-radiative relaxation through molecular vibrations on CD surfaces.^[47] Therefore, we believe both the particle size and the graphitic nitrogen content control the PL emission of our CDs synergistically.



Scheme 1. A possible formation mechanism for CDs with tunable PL emission.

One application of our CDs is to prepare CDs/PVA films with color-tunable emission (Figure 7 and Figure S8, Supporting Information). Under UV light of 365 nm, their emission maxima locate at 441, 513, 572, and 713 nm, respectively, almost the same with those of the original CDs. When the B-CDs, G-CDs, and R-CDs are mixed by a weight ratio of 2:3:2, a pure white-light emissive CDs/PVA composite film with CIE color coordinates of (0.33, 0.33) is obtained dramatically. This white-light emitting film has a QY of 39%, which is remarkable for white-light emitting CDs at present.^[48] The corresponding PL spectrum in Figure 7d exhibits three distinct emission bands, in accordance with the emission peaks of the original CDs/PVA films. This result confirms that there is no significant energy transfer or self-absorption within the CDs mixture.^[22,49] In addition, the photo-stabilities of these CDs/PVA composite films tested under 2 h of UV irradiation are excellent in Figure S9 (Supporting Information). And thus, our color-tunable CDs/PVA composite films are promising candidates for lighting devices.

Another application of our R-CDs is the bioimaging both in vitro and in vivo. Before biological application, the PL properties of the R-CDs in water were measured at first. On one hand, Figure S10 (Supporting Information) show that the R-CDs aqueous solution exhibits the similar optical features with those in ethanol (Figure 2d), and the corresponding QY is as high as 36%. On the other, the luminescence stability of the R-CDs under different conditions was tested and illustrated in Figures S11 and S12 (Supporting Information), which confirm that R-CDs are very stable toward increased ionic strengths and one month storage, respectively. Afterward, standard

3-(4,5-dimethylthiazol-2-yl)-2,5-diphenyltetrazolium bromide (MTT) assays were performed using HeLa cells (Figure S13, Supporting Information), and the results show that the R-CDs are almost nontoxic even at a CDs concentration of up to 400 $\mu\text{g mL}^{-1}$. In the cell imaging experiments (Figure 8a), HeLa cells uptake the R-CDs and show bright red fluorescence in their cytoplasm.^[50] In the mice imaging experiments (Figure 8b), strong fluorescence can be observed at the injection site under excitation of 600 nm and emission of 750 nm, implying that the NIR fluorescence of the R-CDs can efficiently penetrate skin and tissues of mice.^[12] For both in vitro and in vivo imaging experiments, 1 h of continuous laser irradiation cannot weaken the R-CDs fluorescence, indicating that our R-CDs are stable for confocal imaging. As a new kind of fluorescent probes, our R-CDs perform both high photostability and good biocompatibility.

3. Conclusion

In summary, we have developed a facile, controllable, and high-yield approach to synthesize highly efficient excitation-independent CDs with tunable emission over the entire visible range and gradually narrowed FWHM.

We find the choice of reaction solvents, especially the aqueous H_2SO_4 solution, is very important for this approach because the solvents control the dehydration and carbonization processes of precursors, determine the size of sp^2 -conjugated domains and the content of graphitic nitrogen in each CDs sample, and finally lead to different emission colors of CDs from blue to NIR. Our CDs can be dispersed into PVA matrix to be luminescent film with tunable colors, especially the pure white light emission (CIE = 0.33, 0.33, QY = 39%). Our CDs can also act as fluorescent probes for bioimaging both in vitro and in vivo, which are based on their high QY, good photostability and low toxicity in water. Our present work invents a facile route to obtain CDs with excellent optical properties for applications after well understanding and controlling the formation processes of CDs, which also points out a direction for developing highly luminescent CDs with NIR emission windows and narrowed FWHM.

4. Experimental Section

Materials: L-Glutamic acid, o-phenylenediamine, formamide, dimethylformamide, polyvinyl alcohol ($M_w = 96\,500$), and concentrated sulfuric acid (98 wt%) were from Sinopharm Chemical Reagent Co., Ltd. (China). Fetal bovine serum (FBS) and Dulbecco's modified Eagle's medium (DMEM, High Glucose) were from Gibco BRL (USA). MTT and trypsinase were from Sigma-Aldrich. All chemical reagents were used as received without any purification. Ultrapure (Milli-Q) water was used for all experiments.

Synthesis of PL-tunable CDs: The PL tunable CDs were prepared from L-glutamic acid and o-phenylenediamine in a one-pot solvothermal process. For blue to yellow emitting CDs, each couple of L-glutamic acid

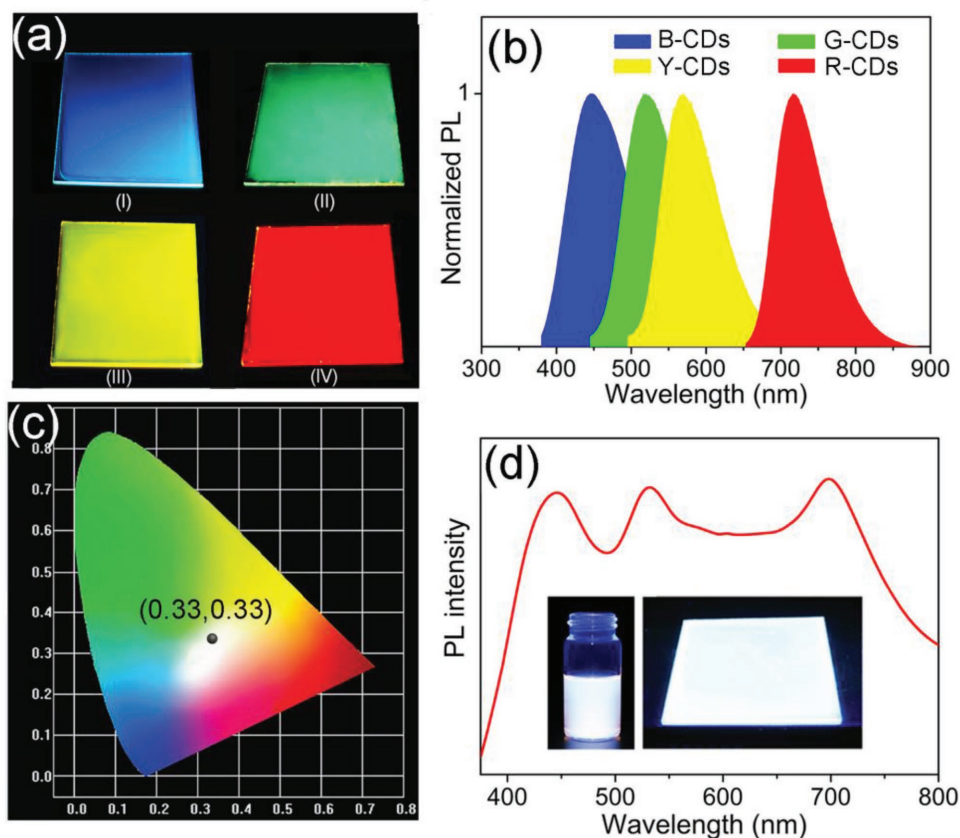


Figure 7. a) Fluorescence images of the (I) B-, (II) G-, (III) Y-, and (IV) R-CDs/PVA composite films on glass substrates under UV light. b) Normalized PL spectra of the B-, G-, Y-, and R-CDs/PVA composite films under 365 nm UV light. c) CIE color coordinate and d) PL spectrum of a white-light emitting CDs/PVA composite film under UV light. The insets in (d) are the photographs of white light emitting CDs solution and CDs/PVA film on glass substrates under UV light.

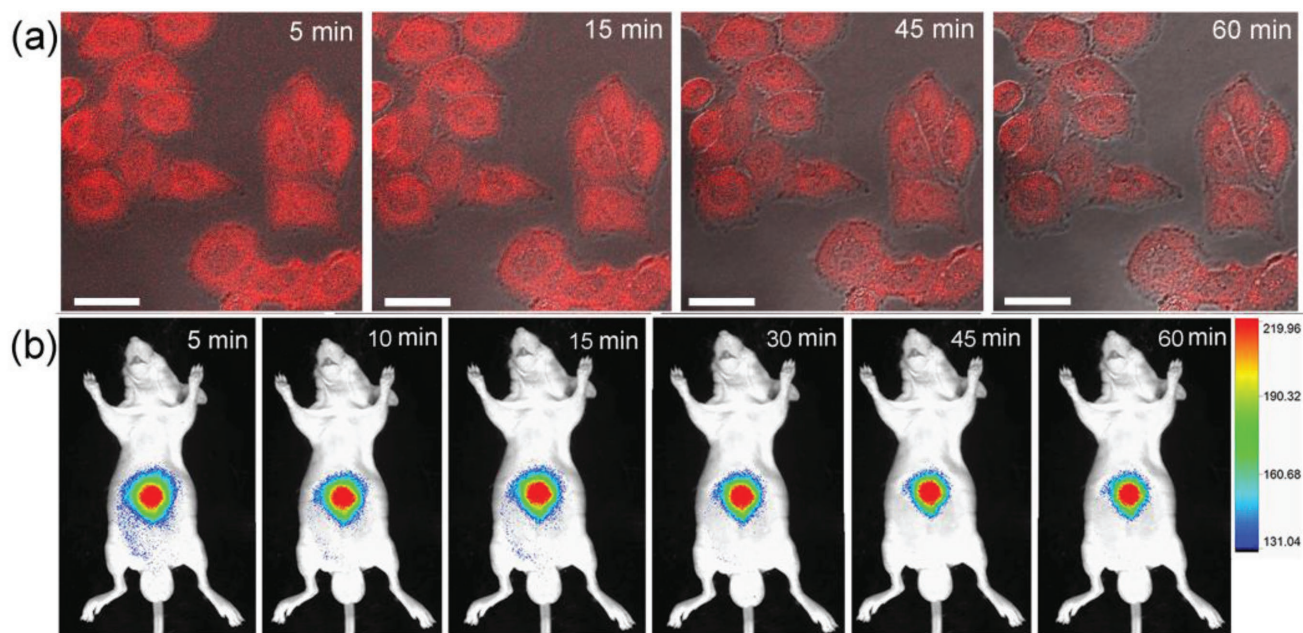


Figure 8. a) Laser scanning confocal microscopy images of HeLa cells labeled by R-CDs aqueous solution ($25 \mu\text{g mL}^{-1}$) with different exposure times. b) In vivo PL images of nude mice after subcutaneous injection of $50 \mu\text{g mL}^{-1}$ of the R-CDs aqueous solution with different exposure times. The white scale bar at the left bottom represents $25 \mu\text{m}$.

(0.11 g) and *o*-phenylenediamine (0.16 g) was dissolved in one kind of mixed solvents (25 mL in total). Such mixed solvents were obtained by mixing formamide and dimethylformamide with volume ratios of 1:0, 1:6, 3:2, and 0:1, respectively. Each solution was transferred into a Teflon-lined stainless-steel autoclave and heated at 210 °C for 10 h. After the reaction finished, each resulting CDs solution was filtered with a membrane (0.22 μm), and then precipitated with a KOH aqueous solution. Finally, the precipitation was obtained by centrifugation at 15 000 r min⁻¹ for 15 min, followed by washing with ethanol/water mixtures for several times, and dried in a vacuum at 40 °C overnight. For orange to NIR emissive CDs, their preparation procedures were almost the same as above, except the solvents. Their solvents were ethanol (99.8 wt%) and diluted sulfuric acid aqueous solution (2.8, 6.1, and 7.3 mol L⁻¹), respectively (see Figure 1).

Fabrication of Full-Color Emissive Films: For the blue/green/yellow/red/white-light emitting films, 2 mL of the corresponding CDs ethanol solution (1.0 mg mL⁻¹) was mixed with 10 mL of PVA aqueous solution (0.08 g mL⁻¹), and then dropped casting on a cleaned glass sheet followed by drying for 1 d under ambient circumstances. Among them, the white light emitting solution was prepared by mixing the B-CDs, G-CDs, and R-CDs with a weight ratio of 2:3:2.

MTT Assays: 100 μL of HeLa cells (with a density of 5 × 10⁴ cells mL⁻¹) were seeded into a 96 well plate in Dulbecco's-modified Eagle's medium (DMEM) with 10% FBS and incubated in an incubator at 37 °C for 24 h. After that, the culture medium was discarded and then 200 μL of DMEM, containing different doses of R-CDs (0–1000 μg mL⁻¹), were added into each well for another 48 h of incubation. Subsequently, 20 μL of 5 mg mL⁻¹ MTT solution was added into each well. After additional 4 h incubation, the growth medium was removed, and 150 μL of DMSO was then added to dissolve the MTT. Finally, the resulting mixture was shaken for 15 min at room temperature. And the optical density of each well was recorded using an automatic enzyme-linked immunosorbent assay (ELISA) Analyzer (SPR-960) at a wavelength of 492 nm.

Cell Imaging: Cellular fluorescence images of R-CDs were captured using a FV10i laser scanning confocal microscope. Typically, 0.5 mL of HeLa cells in DMEM medium with an initial density of 10⁵ cells mL⁻¹ were seeded in 6 well cell culture plates and cultured at 37 °C for 24 h. After incubation, the culture medium was replaced with 1 mL of DMEM medium containing 25 μg mL⁻¹ of R-CDs for 1.5 h of incubation. Finally, the cells were washed three times with phosphate buffered saline to eliminate the free R-CDs and then fixed with 4% paraformaldehyde.

QY Measurements: The quantum yield of the CDs was determined by using an integrating sphere attached to an F-4600 spectrofluorometer. For example, an ethanol solution of the R-CDs was diluted to an optical absorption below 0.1 at excitation wavelength of 634 nm. Then, the obtained ethanol solution was added into a 1 cm fluorescence cuvette, placed in the integrating sphere and excited by 634 nm monochromatic light. Subsequently, the PL spectra were collected in the ranges of 560–950 and 624–644 nm, respectively. Meanwhile, the PL spectra for pure ethanol were also recorded under the same conditions. Finally, the QY of R-CDs was calculated based on PL spectra of both the R-CD sample and pure ethanol using fluorescence software. Each experiment was repeated three times in parallel and the averaged QY of R-CDs was presented. All samples of CDs were measured in the above procedures, and the corresponding conditions and results are listed in Table S1 (Supporting Information).

Characterizations: TEM images of CDs were obtained by a Tecnai G2 F20 transmission electron microscope with a working voltage of 200 kV. The UV–vis absorption spectra were collected on a Shimadzu UV-3101 PC spectrophotometer. The fluorescence spectra was measured on an F-4600 spectrofluorometer with a slit width of 1–2 nm. The Fourier transform infrared spectra were obtained on a Nicolet 380 Infrared spectrometer. The Raman spectra were recorded using a laser confocal micro-Raman spectrometer by excitation of 785 nm. The XRD patterns were performed on a Bruker D8 Advance X-ray diffractometer. The X-ray photoelectron spectra were recorded using a ESCALAB 250Xi Spectrometer (Thermo Fisher). Photoluminescence decay curves were

measured on a QM 40 spectrometer. The photographs of samples were taken by a Canon 760D camera. The in vivo mouse imaging experiments were performed on a Bruker imaging system, under excitation and emission wavelengths of 600 and 750 nm, respectively. The animal protocols of this study were approved by the Institutional Animal Care and Use Committee of the Chinese Academy of Sciences. The animal experiments were performed by strictly following the guidelines and regulations from the Laboratory Animal Centre of Chinese Academy of Sciences (Shanghai, China).

Supporting Information

Supporting Information is available from the Wiley Online Library or from the author.

Acknowledgements

This work was financially supported by the Fundamental Research Funds for the Central Universities (No. 2017QNA08), the National Natural Science Foundation of China (Grant 21771039), the Shanghai Science and Technology Committee (No. 16DZ2270100), and China Postdoctoral Science Foundation (2016M601907).

Conflict of Interest

The authors declare no conflict of interest.

Keywords

carbon dots, controlled synthesis, graphitic nitrogen, photoluminescence, quantum size effect

Received: February 9, 2018

Revised: March 8, 2018

Published online: April 30, 2018

- [1] S. Y. Lim, W. Shen, Z. Gao, *Chem. Soc. Rev.* **2015**, *44*, 362.
- [2] M. Shamsipur, A. Barati, S. Karami, *Carbon* **2017**, *124*, 429.
- [3] X. M. Li, M. C. Rui, J. Z. Song, Z. H. Shen, H. B. Zeng, *Adv. Funct. Mater.* **2015**, *25*, 4929.
- [4] S. Zhu, Y. Song, X. Zhao, J. Shao, J. Zhang, B. Yang, *Nano Res.* **2015**, *8*, 355.
- [5] X. T. Zheng, A. Ananthanarayanan, K. Q. Luo, P. Chen, *Small* **2015**, *11*, 1620.
- [6] Z. L. Wu, Z. X. Liu, Y. H. Yuan, *J. Mater. Chem. B* **2017**, *5*, 3794.
- [7] S. Zhu, Y. Song, J. Wang, H. Wan, Y. Zhang, Y. Ning, B. Yang, *Nano Today* **2017**, *13*, 10.
- [8] F. Yuan, S. Li, Z. Fan, X. Meng, L. Fan, S. Yang, *Nano Today* **2016**, *11*, 565.
- [9] P. Miao, K. Han, Y. Tang, B. Wang, T. Lin, W. Cheng, *Nanoscale* **2015**, *7*, 1586.
- [10] F. Yuan, Z. Wang, X. Li, Y. Li, Z. a. Tan, L. Fan, S. Yang, *Adv. Mater.* **2017**, *29*, 1604436.
- [11] L. Bao, C. Liu, Z. L. Zhang, D. W. Pang, *Adv. Mater.* **2015**, *27*, 1663.
- [12] H. Ding, S. B. Yu, J. S. Wei, H. M. Xiong, *ACS Nano* **2016**, *10*, 484.
- [13] S. Hu, A. Trinchì, P. Atkin, I. Cole, *Angew. Chem., Int. Ed.* **2015**, *54*, 2970.
- [14] W. Liu, C. Li, Y. Ren, X. Sun, W. Pan, Y. Li, J. Wang, W. Wang, *J. Mater. Chem. B* **2016**, *4*, 5772.

- [15] R. Wang, K.Q. Lu, Z. R. Tang, Y. J. Xu, *J. Mater. Chem. A* **2017**, *5*, 3717.
- [16] D. Li, P. Jing, L. Sun, Y. An, X. Shan, X. Lu, D. Zhou, D. Han, D. Shen, Y. Zhai, S. Qu, R. Zboril, A. L. Rogach, *Adv. Mater.* **2018**, *30*, 1705913.
- [17] D. Zhou, Y. Zhai, S. Qu, D. Li, P. Jing, W. Ji, D. Shen, A. L. Rogach, *Small* **2017**, *13*, 1602055.
- [18] L. P. Li, R. P. Zhang, C. X. Lu, J. H. Sun, L. J. Wang, B. T. Qu, T. T. Li, Y. D. Liu, S. J. Li, *J. Mater. Chem. B* **2017**, *5*, 7328.
- [19] Z. Gan, H. Xu, Y. Hao, *Nanoscale* **2016**, *8*, 7794.
- [20] S. Tao, S. Zhu, T. Feng, C. Xia, Y. Song, B. Yang, *Mater. Today Chem.* **2017**, *6*, 13.
- [21] T. Gao, X. Wang, L. Y. Yang, H. He, X. X. Ba, J. Zhao, F. L. Jiang, Y. Liu, *ACS Appl. Mater. Interfaces* **2017**, *9*, 24846.
- [22] K. Jiang, S. Sun, L. Zhang, Y. Lu, A. Wu, C. Cai, H. Lin, *Angew. Chem., Int. Ed.* **2015**, *54*, 5360.
- [23] X. Miao, D. Qu, D. Yang, B. Nie, Y. Zhao, H. Fan, Z. Sun, *Adv. Mater.* **2018**, *30*, 1704740.
- [24] S. Lu, L. Sui, J. Liu, S. Zhu, A. Chen, M. Jin, B. Yang, *Adv. Mater.* **2017**, *29*, 1603443.
- [25] Z. Tian, X. Zhang, D. Li, D. Zhou, P. Jing, D. Shen, S. Qu, R. Zboril, A. L. Rogach, *Adv. Opt. Mater.* **2017**, *5*, 1700416.
- [26] H. Ding, J. S. Wei, H. M. Xiong, *Nanoscale* **2014**, *6*, 13817.
- [27] S. Sun, L. Zhang, K. Jiang, A. Wu, H. Lin, *Chem. Mater.* **2016**, *28*, 8659.
- [28] H. Ding, J. S. Wei, N. Zhong, Q. Y. Gao, H. M. Xiong, *Langmuir* **2017**, *33*, 12635.
- [29] Y. Zhao, X. Wu, S. Sun, L. Ma, L. Zhang, H. Lin, *Carbon* **2017**, *124*, 342.
- [30] Z. Wang, F. Yuan, X. Li, Y. Li, H. Zhong, L. Fan, S. Yang, *Adv. Mater.* **2017**, *29*, 1702910.
- [31] Q. Cui, J. Xu, X. Wang, L. Li, M. Antonietti, M. Shalom, *Angew. Chem., Int. Ed.* **2016**, *55*, 3672.
- [32] Y. Zhang, R. Yuan, M. He, G. Hu, J. Jiang, T. Xu, L. Zhou, W. Chen, W. Xiang, X. Liang, *Nanoscale* **2017**, *9*, 17849.
- [33] S. Khan, A. Gupta, N. C. Verma, C. K. Nandi, *Nano Lett.* **2015**, *15*, 8300.
- [34] F. Ehrat, S. Bhattacharyya, J. Schneider, A. Lof, R. Wyrwich, A. L. Rogach, J. K. Stolarczyk, A. S. Urban, J. Feldmann, *Nano Lett.* **2017**, *17*, 7710.
- [35] M. L. Liu, L. Yang, R. S. Li, B. B. Chen, H. Liu, C. Z. Huang, *Green Chem.* **2017**, *19*, 3611.
- [36] Q. Chang, X. Han, C. Xue, J. Yang, S. Hu, *Chem. Commun.* **2017**, *53*, 2343.
- [37] Y. Dong, Y. Chen, X. You, W. Lin, C. H. Lu, H. H. Yang, Y. Chi, *Nanoscale* **2017**, *9*, 1028.
- [38] Y. Dong, H. Pang, H. B. Yang, C. Guo, J. Shao, Y. Chi, C. M. Li, T. Yu, *Angew. Chem., Int. Ed.* **2013**, *52*, 7800.
- [39] H. Ding, Y. Ji, J. S. Wei, Q. Y. Gao, Z. Y. Zhou, H. M. Xiong, *J. Mater. Chem. B* **2017**, *5*, 5272.
- [40] C. Wang, K. Jiang, Q. Wu, J. Wu, C. Zhang, *Chem. - Eur. J.* **2016**, *22*, 14475.
- [41] H. Nie, M. Li, Q. Li, S. Liang, Y. Tan, L. Sheng, W. Shi, S. X. A. Zhang, *Chem. Mater.* **2014**, *26*, 3104.
- [42] S. Zhu, Q. Meng, L. Wang, J. Zhang, Y. Song, H. Jin, K. g. Zhang, H. Sun, H. Wang, B. Yang, *Angew. Chem., Int. Ed.* **2013**, *52*, 3953.
- [43] L. Guo, J. Ge, W. Liu, G. Niu, Q. Jia, H. Wang, P. Wang, *Nanoscale* **2015**, *8*, 729.
- [44] K. Hola, M. Sudolska, S. Kalytchuk, D. Nachtigallova, A. L. Rogach, M. Otyepka, R. Zboril, *ACS Nano* **2017**, *11*, 12402.
- [45] X. Li, Z. Zhao, C. Pan, *Chem. Commun.* **2016**, *52*, 9406.
- [46] D. X. Ye, Y. Y. Ma, W. Zhao, H. M. Cao, J. L. Kong, H. M. Xiong, H. Möhwald, *ACS Nano* **2016**, *10*, 4294.
- [47] S. Bhattacharyya, F. Ehrat, P. Urban, R. Teves, R. Wyrwich, M. Doblinger, J. Feldmann, A. S. Urban, J. K. Stolarczyk, *Nat. Commun.* **2017**, *8*, 1401.
- [48] J. He, Y. He, Y. Chen, B. Lei, J. Zhuang, Y. Xiao, Y. Liang, M. Zheng, H. Zhang, Y. Liu, *Small* **2017**, *13*, 1700075.
- [49] D. Zhou, D. Li, P. Jing, Y. Zhai, D. Shen, S. Qu, A. L. Rogach, *Chem. Mater.* **2017**, *29*, 1779.
- [50] J. H. Liu, L. Cao, G. E. LeCroy, P. Wang, M. J. Meziani, Y. Dong, Y. Liu, P. G. Luo, Y. P. Sun, *ACS Appl. Mater. Interfaces* **2015**, *7*, 19439.